RSC Advances

ROYAL SOCIETY OF CHEMISTRY

www.rsc.org/advances

Ohmic Contact of Indium Oxide as Transparent Electrode to n-type Indium Phosphide

Xiufeng Tang[a,b,*], Chunhan Hseih[a], Fang Ou[a] and Seng-Tiong Ho[a]

[a] *Department of Electrical Engineering and Computer Science, Northwestern University, Evanston, Illinois 60208, United States*

[b] *State Key Laboratory of Solidification Processing, School of Materials Science and Engineering, Northwestern Polytechnical University, Xi'an 710072, China;*

* Corresponding author. Tel.: (+86) 029-88494574;

E-mail address:

Xiufeng Tang: tbrenda@sina.com

Chunhan Hseih: chunhanhseih2013@u.northwestern.edu

Seng-Tiong Ho: sth@northwestern.edu

Abstract

Ohmic contacts to n-type indium phosphide (n-InP) with indium oxide (In_2O_3), a transparent conducting oxide (TCO), have been achieved. Hydrogen plasma surface pretreatment of the n-InP substrates (H_2-cleaned n-InP) prior to the deposition of In_2O_3 films, is the key to achieve Ohmic contact. Oxygen flow rate during the In_2O_3 film deposition, which equivalently determines its doping level, is the main tuning parameter for In_2O_3 thin films growth. Rapid thermal annealing process (RTP) at different temperatures was found to have little effects on the Ohmic contact type.

Keywords: Ohmic contact, In_2O_3 thin film, n-type InP, surface pretreatment, annealing process

1. Introduction

Transparent high-conductivity Ohmic contacts are of primary importance for optoelectronic devices, such as high electron mobility transistors [1], light emitting diodes (LEDs) [2] and solar cells [3]. Although the large band gaps usually associated with optical transparency preclude the possibility of high conductivity in many transparent materials, a number of metal oxides, known as transparent conducting oxides (TCOs), possess the unique properties of being both transparent and highly conductive [4].

Compared with the majority of TCOs, indium oxide (IO) as a binary compound TCO does not need extrinsic doping and has the advantage of ease of tuning the chemical composition during film deposition. What's more, the superiority of IO films over tin oxide (SnO_2) films as transparent electrodes is largely due to the higher mobility in IO [5]. IO films prepared by various techniques have mobility in the range of 10-75 $cm^2\ V^{-1}\ s^{-1}$, with carrier concentration around 10^{19}-10^{20} cm^{-3} [5]. The optical transmittance of IO films in the visible and near-IR regions is about 75%-90% [6-8]. Additionally, the refractive index of IO films in the visible region ranges between 1.9 and 2.08 [8, 9]. The low refractive index of IO relative to InP ($n\approx3.2$) also possesses the possibility that IO could be used as a conducting waveguide cladding material for current injection into high refractive index contrast nanophotonic devices [10, 11]. A critical concern for these applications, however, is the electrical properties across the interface between the IO films and InP substrates. The contact should be Ohmic

and the resistance should be minimized [12, 13].

Generally, in order to achieve Ohmic contact between a TCO film and an n-type nondegenerate semiconductor, it is required that the Fermi level of the TCO ($ø_{IO}$) be less than that of the semiconductor ($ø_{InP}$) [14, 15]. For the donor-doped n-InP substrates used in this study ($n=7.00\times10^{17}$ cm^{-3}), the Fermi level (E_F) is estimated to be 0.39 eV below the conduction band minimum (E_c) by using Equation 1, shown as follows,

$$E_F = E_c - k_b T \cdot \ln(\frac{n}{n_i}) \qquad \textbf{(1)}$$

where k_b is the Boltzmann constant; T is the room temperature (300 K); n_i is the intrinsic carrier concentration of InP as 1.317×10^7 cm^{-3} [16]. We know that the work function is defined as the energy difference between the vacuum level and the Fermi level, which for an n-type semiconductor can be also written as $x + (E_c-E_F)$. Therefore, $ø_{InP}$ is estimated to be 4.77 eV, where the electron affinity x of InP is 4.38 eV [16]. For In_2O_3 films, the work function was reported as 4.6-4.7 eV for as-deposited films by D.C. magnetron sputtering [17], 4.88 eV and very close to 5 eV for films prepared by means of reactive evaporation [7,18,19]. But In_2O_3 film still poses great possibility to form Ohmic contact to n-InP. First, we know the work function of In_2O_3 films depends critically on the preparation method and process parameters. Second, in our study, in order to achieve Ohmic contact between the In_2O_3 film and the n-InP substrate, H_2 or O_2 plasma surface pretreatments were done on n-InP substrates, which have been verified to change the effective surface work function of ITO [20-22].

Actually, our previous results [23] have shown that Ohmic contact of CdO to n-InP can be achieved by eliminating the interfacial oxide layer with H_2 plasma surface treatment on the substrate prior to film deposition and low interfacial contact resistance of $(6.8\pm2.8)\times10^{-6}$ $\Omega\cdot cm^2$ was obtained. However, CdO is toxic and pose a great threat to the environment. In_2O_3 is a promising alternative to form Ohmic contact to n-InP.

In this paper, we present results for optical and electrical properties of indium oxide (In_2O_3) thin films deposited by ion beam assisted deposition (IAD). The electrical contact properties across the interface between the contact material, In_2O_3, and the semiconductor, n-InP are investigated. The oxygen partial pressure during deposition is the main tuning parameter for In_2O_3 films growth. Effects of oxygen partial pressure during deposition on microstructure and surface morphology, grain size and surface roughness, optical and electrical properties of In_2O_3 films were ever systematically reported [24-26]. While, in our study, In_2O_3 films will be used as cladding electrodes and therefore optical and electrical properties of bulk In_2O_3 films and especially the interfacial electrical contact properties are our big concern. In addition, we know, in InP based photonic device fabrication, rapid thermal annealing processes (RTP) are often required. So, it is also necessary to investigate what effect RTP would have on the interfacial contact properties between In_2O_3 and InP.

2. Experimental

2.1 Film preparation

In_2O_3 thin films were prepared at room temperature using Ion-Assisted Deposition (IAD, ION TECH, INC, USA) with In_2O_3 target (99.99% pure, Kurt J. Lesker company). IAD consists of a main ion source and an assisted ion source. The main beam will sputter out In_2O_3 from the target, while the assistant beam directed toward the substrate will provide additional kinetic energy to the sputtered In_2O_3, increasing the film surface energy without further heating. Therefore, thin films prepared by IAD possess good adhesiveness without additional substrate heating. In addition, cooling water running in the back of the sample further stabilizes the local temperature during deposition and does not exceed 50℃.

Properties of In_2O_3 are strongly dependent on its doping level, which are mainly oxygen vacancies. The oxygen partial pressure, which is controlled by the oxygen flow rate of the assistant beam during deposition, is therefore the main tuning parameter for In_2O_3 thin films growth. Oxygen flow rates of 0 sccm, 3 sccm, 5 sccm, and 7 sccm were used and the deposited corresponding thin films are referred to as In_2O_3-0, In_2O_3-3, In_2O_3-5, and In_2O_3-7 respectively. Deposition time is 60 min and the working pressure is 4.5×10^{-4} Torr. The film thickness is about 100 nm, which is tested by an alpha-step 200 from Tencor Instruments. Other detailed parameters of In_2O_3 deposition are listed in Table 1.

2.2 Bulk In_2O_3 properties measurement

Bulk material properties of In_2O_3 were characterized using thin films deposited on commercial glass slides. Electrical properties were carried out using Hall Effect

measurements with films of Van der Pauw geometry. For optical properties, transmittance and reflectance spectra were measured in the spectral range from 200 nm to 2000 nm using a UV/Vis/IR Perkin-Elmer lambda 1050 spectrophotometer with the integrating sphere in the dual beam mode. Microstructure of the as-deposited In_2O_3-3 film was examined using scanning electron microscope (SEM, Hitachi S4800) and an RIGAKU: ATX-G x-ray diffractometer .

2.3 Contact patterns fabrication and Electrical contact properties measurement

Interfacial properties are characterized using the In_2O_3 thin films deposited on n-type InP substrates ($n=7.00\times10^{17}cm^{-3}$). Prior to deposition, all InP substrates were first solvent cleaned in 3 minutes of ultrasonic bath sequentially in acetone, IPA (Isopropyl Alcohol), and then deionized water; substrates cleaned by this method are referred to as solvent-cleaned samples. Some substrates were further cleaned by reactive ion etching (RIE) in Oxygen and others in Hydrogen (O_2 or H_2, 50 mtorr, 100 W, 1 min). Samples received surface treatments of RIE plasma cleaning are referred to as O_2-cleaned or H_2-cleaned. It should be noted that all samples were directly put into IAD apparatus right after ex-situ pretreatments. B. Anthony's study [27] showed that H plasma clean can protect the wafer from contamination for up to 15 min in ambient air. So measures were taken to shorten the elapse to be less than 10 min.. ANTHONY

In order to examine the electrical contact properties, photolithography process was used

to define contact patterns for transmission line method measurements. Fabrication process flow is shown in Fig.1: linear arrays of 200 um by 200 um square pads with various gap distances apart (10-60 um gap in 10 um increment). Ti/Au (10 nm/300 nm) was then deposited by E-beam evaporation followed by a lift-off process to form metal contacts on In_2O_3. Finally, using the deposited metal pads as a self-alignment mask, the exposed In_2O_3 film was removed using RIE in Methane/H_2/Ar gases (CH_4:H_2:Ar=10:30:10 sccm, 50 mtorr, 200 W) to complete the fabrication process. The electrical current-voltage characteristics between In_2O_3 films and InP substrates were measured by standard two-probe measurement method using a Kiethley 2400 source meter.

2.4 Annealing heat treatments detail

The annealing treatments were carried out using a Jet First 100/150 Rapid Thermal Process, at 360 ℃, 400 ℃ and 450 ℃, which are the temperatures chosen for device contact annealing. The annealing duration is 60 seconds, while the temperature was raised rapidly in 10 seconds in forming gas (20% H_2, balance N_2).

3. Results and discussion

3.1 Properties of bulk In_2O_3

The measured electrical and optical properties of bulk In_2O_3 are concisely summarized in Table 2. From Table 2, we can tell with increasing the O_2 flow rate during the film deposition, the carrier concentration decreases from 8.53×10^{19} to 2×10^{17}cm^{-3}. Higher oxygen partial

pressure during film deposition results in lower carrier concentration due to the reduction of oxygen vacancies. The Hall mobility of In_2O_3 ranges from 13.1~29.3 $cm^2/V{\cdot}s$; the conductivity is highest at 355.5 S/cm for In_2O_3-0, while for In_2O_3-7 the conductivity is as small as 0.71 S/cm, which indicates that In_2O_3-7 is highly oxidized and low in oxygen vacancies.

We know that fiber-optic communication transmission windows around 1500 nm are most widely-used, which have the lowest attenuation losses and achieve the longest range. Therefore, in this study, the optical constants (refractive index n and absorption coefficient k) at 1550 nm are extracted from the transmittance and reflectance spectra, shown in Fig.2, corrected by the substrate transmittance and reflectance spectra employing the interference pattern resulted from multiple reflections in the film and the glass substrate. From Fig.2, we know that the optical transmittance of In_2O_3 in the visible and near-IR regions is about 75%-90%, which is consistent with reported data [6, 7]. The high optical transparency of In_2O_3 in the visible and near-IR regions is a direct consequence of its wide band gap (Eg ~ 3.0 eV) [28]. Additionally, the fundamental absorption edges of In_2O_3 generally lie in the UV and shift to shorter wavelengths with lower O_2 flow rate, due to the increasing carrier concentration. The refractive index in the visible region increases from 1.84 to 2.01 in dependence of the increasing O_2 flow rate during the deposition, because of the more sufficient oxidation. Optical loss at 1550 nm is highest for In_2O_3-0 at 2061cm^{-1} and lowest for

In_2O_3-7 at 320.7cm^{-1}, where higher loss at higher carrier concentration results from free carrier absorption and free carrier scattering.

The optical band gap of In_2O_3 is estimated using the graph of $(\alpha h\nu)^2$ versus $h\nu$ [29] (as shown in Fig.3), where α, the optical attenuation coefficient at energy $h\nu$, is extracted from the transmittance and reflectance spectra using the relation $\alpha = -(1/d)\log(T/(1-R))$, where *d* is the film thickness. From Fig.3, we can tell the optical band gap increases with the increasing carrier concentration. The optical band gap energy depends on the carrier concentration as a result of the band filling effect, also known as the Burstein-Moss shift [30]: the filling of excessive carrier in the conduction band leads to the increase of the optical band gap energy. To sum up, a trade-off relation is indicated for the engineering of the conductivity and the optical loss of bulk In_2O_3 thin films.

3.2 Microstructure of In_2O_3 films

SEM and XRD spectrum of the as-deposited In_2O_3-3 film was shown in Fig.4. The SEM result shows that the as-deposited film prepared by IAD is smooth and dense with grain size about 50 nm. And the XRD result shows that the as-deposited film is already polycrystalline, but some amorphous contribution can not be excluded. Structures comprising amorphous and polycrystalline components are common for In_2O_3 films annealed or processed below 200 ℃ [31]. Regarding In_2O_3, the film exhibits sharp crystalline peaks, which clearly correspond to the cubic structure of the mineral bixbyite ((JCPDS 6-0416). For In_2O_3, deposited at low

temperature, the predominant planes are (222) and (400) [32], which is the case here. A (100) or (111) preferred orientation has generally been reported in In_2O_3 films which have been obtained by various techniques [8, 33, 34].

3.3 Interfacial electrical contact property

For interfacial electrical contact experiments, contacts to n-type InP substrates pretreated with standard solvent cleaning, O_2 cleaning and H_2 cleaning, from thin films of In_2O_3-0, In_2O_3-3, In_2O_3-5, and In_2O_3-7, were examined. Fig.5 shows I-V curves of the In_2O_3 contact to n-InP of different O_2 flow rates during In_2O_3 deposition: (a) solvent-cleaned n-InP substrates; (b) O_2-cleaned n-InP substrates; (c) H_2-cleaned n-InP substrates. For solvent-cleaned substrates as shown in Fig.5 (a), Ohmic contact is shown for n-InP to In_2O_3-0 and In_2O_3-3 thin films, while Schottky behavior is shown for In_2O_3-5, and In_2O_3-7 contacts to n-InP. The difference in carrier concentration results in different Fermi energy and work function of the In_2O_3 films, whereas the energy bands are predominately aligned for less oxidized, films with higher carrier concentration forming the Ohmic contact. However, for O_2 plasma cleaned substrates, all film contacts to n-InP show Schottky behavior (seen in Fig.5 (b)). This implies that an interfacial oxide layer might exist between the film and the substrate for O_2 plasma pretreated samples [23]. If such oxide layer exists and causes the Schottky behavior, the removal of such layer could allow the formation of Ohmic contact. Then some substrates were treated by H_2 plasma after standard solvent cleaning prior to In_2O_3 film deposition. The

contact measurements of those samples are shown in Fig.5 (c). All In_2O_3 films form Ohmic contact to n-InP substrates pre-treated using H_2 plasma.

Dynamic resistances of In_2O_3 film contacts to H_2-cleaned InP substrates in terms of different O_2 flow rates during film deposition are listed in Fig.6, which are calculated from the I-V curves such as those in Fig.5 (c). It can be seen that the dynamic resistance shows a decreasing trend with the increasing O_2 flow rate. It should be noted that besides the In_2O_3 film resistance and the In_2O_3/InP contact resistance, the dynamic resistance as calculated from I-V curves is the total resistance also including the resistances due to the probes, the metal pads, the InP substrate, and the probe/metal and the metal/ In_2O_3 interfaces but these resistances are not affected by the increasing O_2 flow rate and the hydrogen pretreatment. In consideration of the decreasing conductivity of the In_2O_3 films with the increasing O_2 flow rate, seen in Table 2, we can conclude that the dynamic In_2O_3/InP interfacial contact resistance decreases with tuning the O_2 flow rate from 0 sccm to 7 scccm, after hydrogen pretreatment. On the other hand, comparing with the dynamic resistances of In_2O_3-0 and In_2O_3-3 films contacts to solvent-cleaned InP substrates calculated from Fig.5 (a) as 2.46 Ω and 2.78 Ω separately, the dynamic resistances of those films contacts to H_2-cleaned InP substrates are 2.12 Ω and 2.07 Ω separately, as shown in Fig.6. It means that the hydrogen plasma pretreatment is not only crucial for In_2O_3 films to form Ohmic contact with n-InP substrates but also good for improving the interfacial conductivity of the In_2O_3/InP contact.

Fig.7 (a) shows the I-V curve measurements of the In_2O_3 -3 contacts to H_2-pretreated n-InP substrates in terms of different post-deposition rapid thermal processes (RTP) to investigate whether the annealing process will affect the ohmic contact property. It can be seen that the contact properties between In_2O_3 and n-InP remain to be Ohmic after all the annealing heat treatments at 360 ℃, 400 ℃ and 450 ℃. This might be due to the carrier concentration remains unchanged (mainly oxygen vacancies). Meanwhile, the dynamic resistance of the In_2O_3-3 film/n-InP substrate samples were calculated, as plotted in Fig.7 (b). Comparing with that of the as-deposited sample at 2.07 Ω, the dynamic resistance first increases slowly to 2.3 Ω when the annealing temperature is lower than 400 ℃ and then increases sharply to 3.3 Ω with the temperature increased to 450 ℃. Effects of annealing heat treatments at various temperatures, in different atmosphere or for different duration time on electrical properties of In_2O_3 films were ever investigated [35-37]. Especially, Yuan's study of annealing on In_2O_3 films in vacumm [35], Oh's study of annealing on Al-doped ZnO films in H_2 atmophere [38] and Lin's study of annealing on In_2O_3:Sn films in N_2 atmosphere [39] have shown that grain size will increase and crystallite quality will be promoted after annealing process and the resistivity of bulk films will decrease, either due to the grain boundary scattering mechanism[35] or originating from the desorption of the negatively charged oxygen species from the grain boundary surfaces by the hydrogen treatment [38]. So resistivity of bulk In_2O_3 films will get lower after annealed in H_2+N_2 atmosphere. What is

more, besides the bulk In_2O_3 film resistance and the In_2O_3/InP contact resistance, the dynamic resistance includes resistance due to the probes, the metal pads, the InP substrate, and the probe/metal and the metal/ In_2O_3 interfaces that remains as a constant. Therefore, we can conclude that the In_2O_3/InP interfacial contact resistances first increase slowly with the increasing annealing temperature and then change sharply when the annealing temperature is high at 450 ℃, which can be probably explained by the interfacial diffusion.

All results show that though the Ohmic contact of In_2O_3 to n-InP is not only compatible to RTP but also the RTP is good for improving the quality of In_2O_3 films, the conductivity of the In_2O_3/InP contacts will deteriorate drastically when the annealing temperature is too high, suggesting that choosing optimal annealing temperature is important in device contact heat treatments.

4. Conclusions

Ohmic contact of In_2O_3 thin films prepared by IAD to n-type InP can be achieved with H_2 plasma pre-treated substrates, which isn't obviously affected by tuning the oxygen flow rate during the film deposition or the post-deposition rapid thermal annealing processes. For optical and electrical properties, by tuning the ambient oxygen pressure during the film deposition, we obtained In_2O_3 films with low optical loss (lowest at 320.7 cm^{-1} for In_2O_3-7) at the 1550 nm wavelength range and reasonable conductivity (highest at 355.5 S/cm for In_2O_3-0). These results indicate the promising potential of In_2O_3 thin films as transparent

electrodes for designing InP based optoelectronic devices for optical communication applications.

Acknowledgements

This work was partially made possible through financial support from the Northwestern IGERT fellowship grant. Use of the Center for Nanoscale Materials clean room of Argonne National Lab was supported under proposal number CNM30847.

References

[1] Dawson, D., Samoska, L., Fung, A. K. and etc. Microwave Wireless Compon.Lett. 2005, 15, 874-876.

[2] Liu, Y. J., Yen, C. H., Hsu, C. H., and etc. Opt. Rev. 2009, 16, 575-577.

[3] Van de Lagemaat, J., Park, N. G., Frank, A. J. J. Phys. Chem. B 2000, 104, 2044-2052.

[4] Tadatsugu Minami, New n-Type Transparent Conducting Oxides, Mrs Bulletin/August, 2000, 38-44.

[5] K. L. Chopra, S. Major and D. K. Pandya, Thin Solid Films, 1983, 102, 1-46.

[6] S. Noguchi and H. Sakata, .I. Phys. D, 1980, 13, 1129.

[7] C.A. Pan and T. P. Ma, Appl. Phys. Lett. 1980, 37, 163.

[8] C.E. Wickersham and J. Greene. Phys. Status Solidi A, 1978, 47, 329.

[9] H.K. Muller, Phys. Status Solidi, 1968, 27, 723.

[10] Nunoya, N. Nakamura, M., Morshed, M., Tamura, S., Arai, S.IEEE J. Sel. Top. Quant. Electron. 2001, 7, 249-258.

[11] Minami, T Semicond. Sci. Technol. 2005, 20, S35-S44.

[12] Chen, K. J., Enoki, T., Maezawa, K., Arai, K., Yamamoto, M.IEEE Trans. Electron Devices 1996, 43, 252-257.

[13] Lin, H. C., Senanayake, S., Cheng, K. Y., Hong, and etc. P. IEEE Trans. Electron Devices 2003, 50, 880-885.

[14] Blank,T.V.; Gol'dberg, Y.A. Semiconductors 2007, 41, 1281-1308.

[15] Wang, S. Fundamentals of Semiconductor Theory and Device Physics; Prentice Hall,

[16] Physical Properties of Semiconductors, Ioffe Physico-Technical Institute. http://www.ioffe.ru/SVA/NSM/Semicond/index.html.

[17] David S. Ginley, Handbook of Transparent conductors, P160.

[18] V. Korobov, M. Leibovitch, and Yoram Shapira. J. Appl. Phys., 1993, 74, 3251-3256.

[19] A. Golan, J. Bregman, Y. Shapira, and M. Eizenberg. Appl. Phys. Lett., 1990, 57, 2205-2207.

[20] Carrie Donley, Darren Dunphy, David Paine, and etc. Langmuir 2002, 18, 450-457.

[21] Milliron, F. J.; Hill, I. G.; Shen, C.; Kahn, A.; Schwartz, J. J. Appl. Phys. 2000, 87, 572-576.

[22] Wu, C. C.; Wu, C. I.; Sturm, J. C.; Kahn, A. Appl. Phys. Lett. 1997, 70, 1348-1350.

[23] Fang Ou, D. Bruce Buchholz, Fei Yi and etc. ACS Appl. Mater. Interfaces 2011, 3, 1341-1345.

[24] A. Golan, J. Bregman, and Y. Shapira and M. Eizenberg. Appl. Phys. Lett. 1990, 57, 2205-2207.

[25] V. Korobov and Yoram Shapira, B. Ber, K. Faleev and D. Zushinskiy. J. Appl. Phys. 1994, 75 (4), 2264-2269.

[26] Sreejith Karthikeyan, Arthur E. Hill and Richard D. Pilkington. Thin Solid Films 2014,

550, 140-144.

[27] B. Anthony, T. Hsu, L. Breaux, R. Qian, S. Banerjee and A. Tasch, Journal of Electronic Materials, 1990, 19 (10): 1027-1032.

[28] Junqiao Wu，Jinbo Cao，Wei-Qiang Han, Functional Metal Oxide Nanostructures，P136.

[29] P. Prathap, Y.P.V. Subbaiah, M. Devika, K.T. Ramakrishna Reddy, Materials Chemistry and Physics, 2006, 100, 375-379.

[30] E. Burstein, Phys. Rev., 1954, 93, 632.

[31] Rodrigo Martins，Elvira Fortunato，Pedro Barquinha，Luis Pereira, Transparent Oxide Electronics: From Materials to Devices, P19.

[32] J.F. Wager, D.A. Keszler, and R.E. Presley (2008) Transparent Electronics. New York: Springer.

[33] P. Nath, R. F. Bunshah, B. M. Basol and O. M. Staffsud, Thin Solid Films, 1980, 72, 463.

[34] V.M. Vainshtein and V. I. Fistul, Sov. Phys.--Semicond., 1967, 1, 104.

[35] Zijian Yuan, Xiaming Zhu, Xiong Wang and etc. Thin Solid Films 2011, 519, 3254-3258.

[36] Kazuhiro Kato, Hideo Omoto, Takao Tomioka and Atsushi Takamatsu. Thin Solid Films 2011, 520, 110-116.

[37] T. Suzuki, T. Yamazaki, M. Takizawa, O. Kawasaki. Journal of Materials Science 1989, 24, 187-191.

[38] Byeong-Yun Oh, Min-Chang Jeong, Doo-Soo Kim and etc. Journal of Crystal Growth 2005, 281, 475-480.

[39] Limei Lin, Fachun Lai, Yan Qu and etc. Materials Science and Engineering B 2007, 138, 166-171.

Figure Captions:

Fig.1 Schematic representation of the fabrication process used to define the electrical contact measurement pattern

Fig.2 Transmittance and reflectance spectra of In_2O_3-0, In_2O_3-3, In_2O_3-5 and In_2O_3-7

Fig.3 Graph of $(\alpha h\nu)^2$ versus photon energy(eV)

Fig.4 SEM and XRD spectra of the as-deposited In_2O_3-3 film

Fig.5 I-V curve measurements of the In_2O_3 contacts to n-InP of different O_2 flow rates during film deposition: (a) solvent-cleaned n-InP substrates; (b) O_2-cleaned n-InP substrates; (c) H_2 -cleaned n-InP substrates

Fig.6 Dynamic resistances of In_2O_3 film contacts to H_2-cleaned n-InP substrates in terms of different O_2 flow rates

Fig.7 In_2O_3-3 contacts to H_2-cleaned n-InP substrates in terms of different post-deposition annealing temperatures, (a) I-V curve measurements; (b) Calculated dynamic resistances

Table 1 Parameters of In_2O_3 films deposition by IAD

Table 2 Bulk material properties of In_2O_3 at different deposition conditions

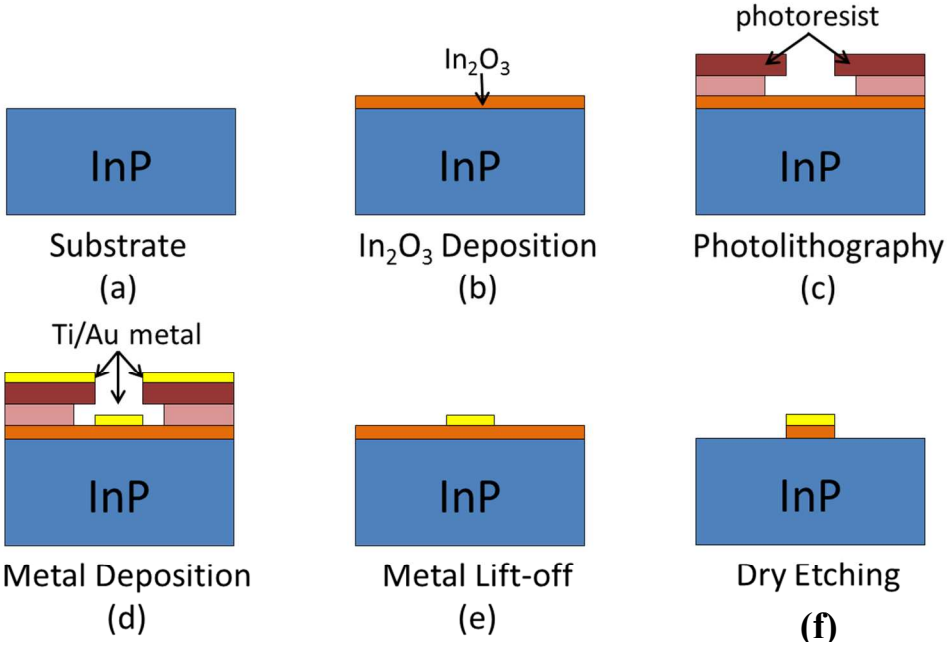

Fig.1 Schematic representation of the fabrication process used to define the electrical contact measurement pattern

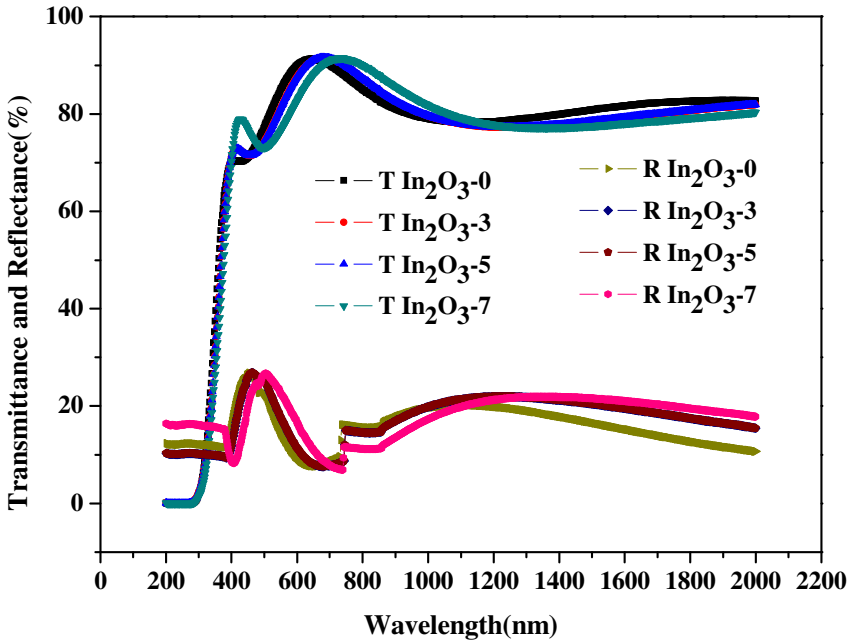

Fig.2 Transmittance and reflectance spectra of In_2O_3-0, In_2O_3-3, In_2O_3-5 and In_2O_3-7

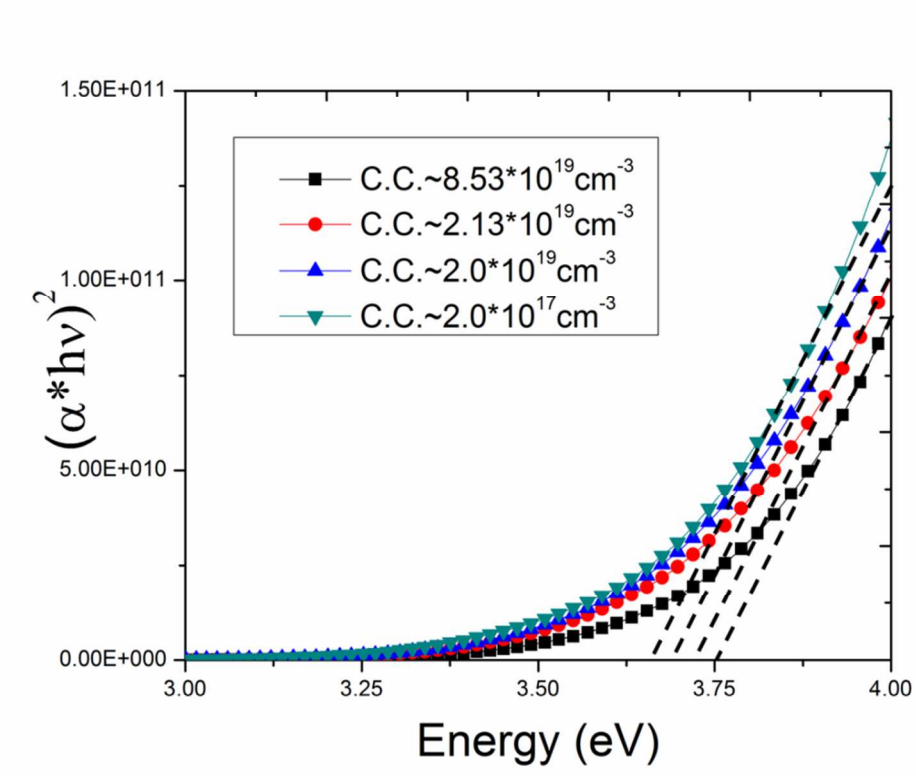

Fig.3 Graph of $(\alpha h\nu)^2$ versus photon energy(eV)

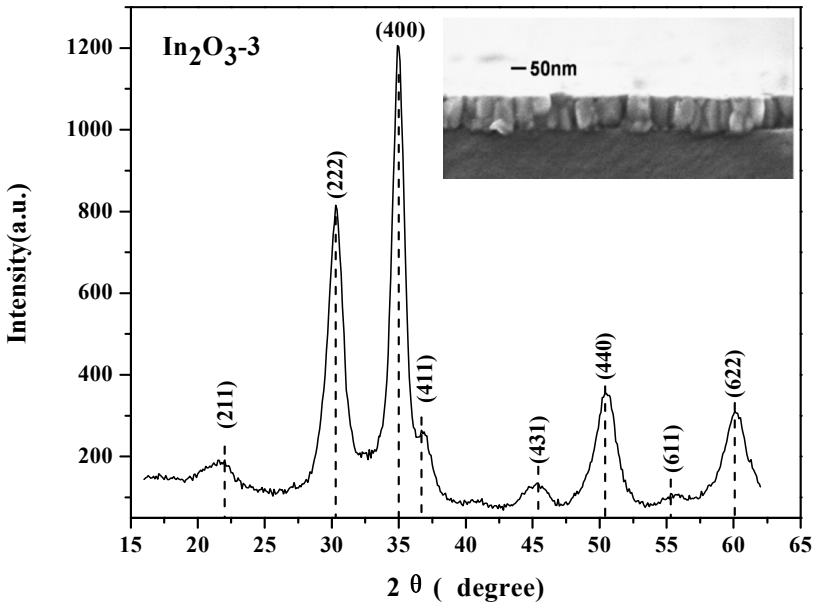

Fig.4 SEM and XRD spectra of the as-deposited In_2O_3-3 film

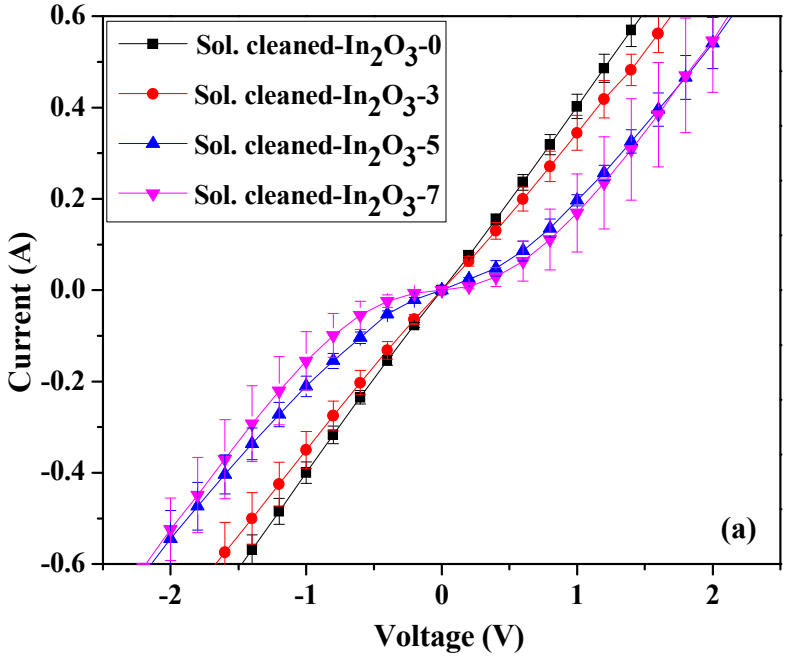

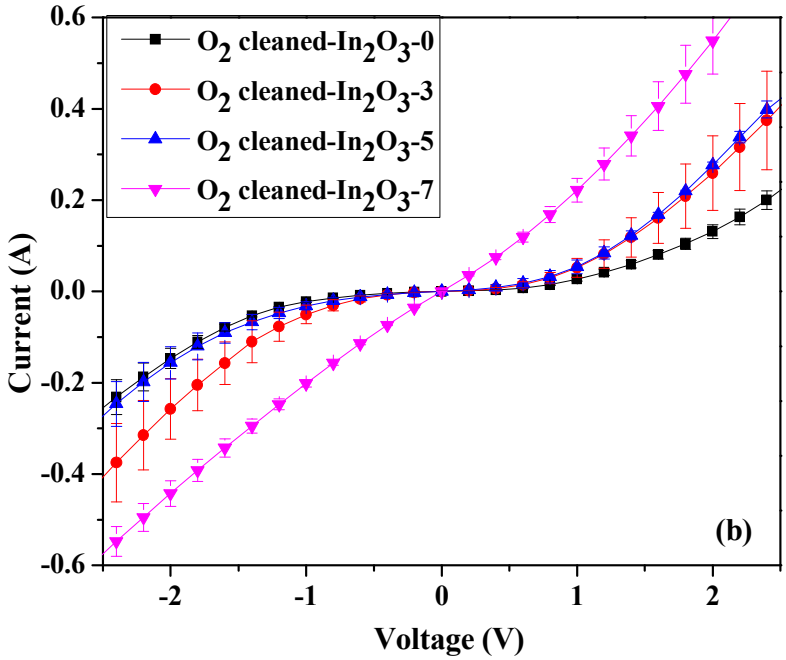

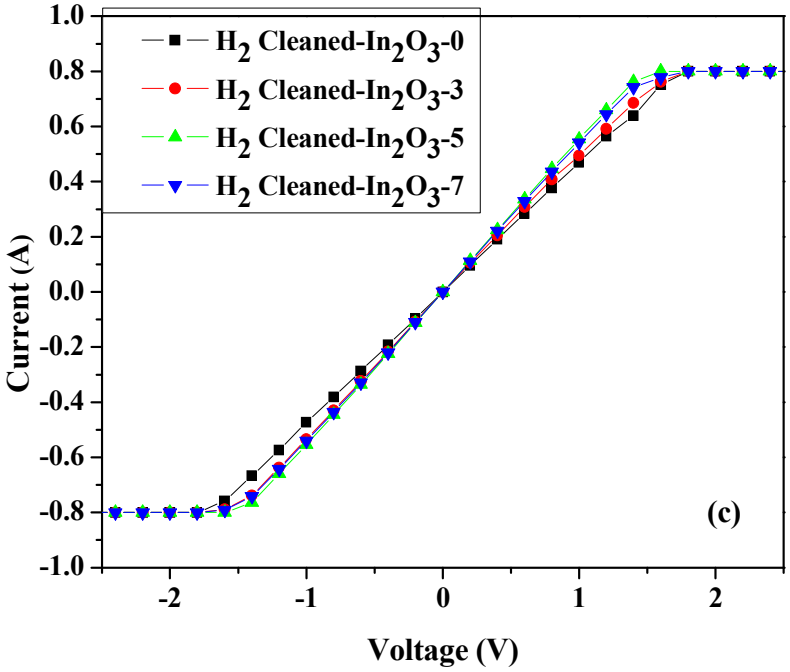

Fig.5 I-V curve measurements of the In_2O_3 contacts to n-InP of different O_2 flow rates during film deposition: (a) solvent-cleaned n-InP substrates; (b) O_2-cleaned n-InP substrates; (c) H_2 -cleaned n-InP substrates

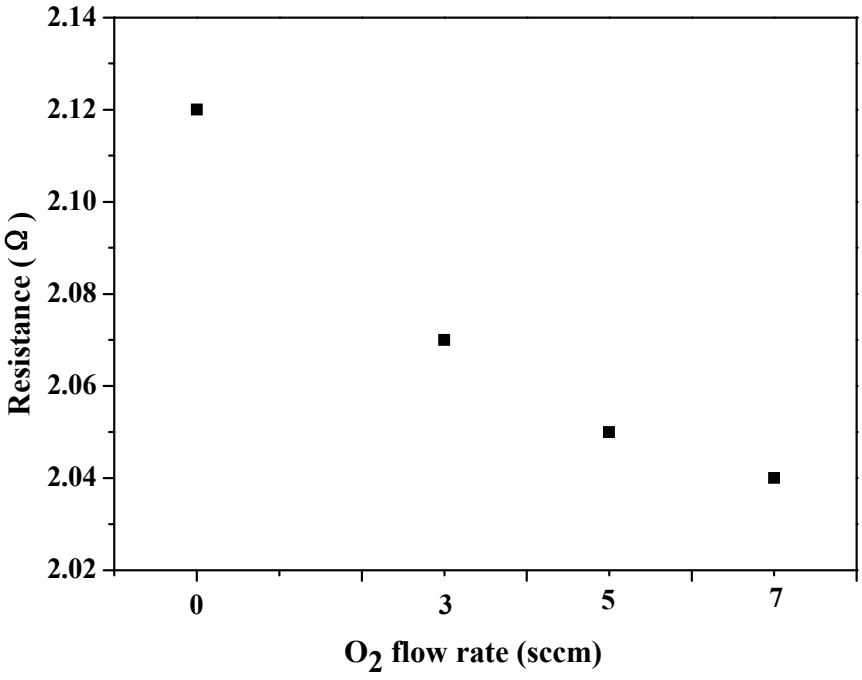

Fig.6 Dynamic resistances of In_2O_3 film contacts to H_2-cleaned n-InP substrates in terms of different O_2 flow rates

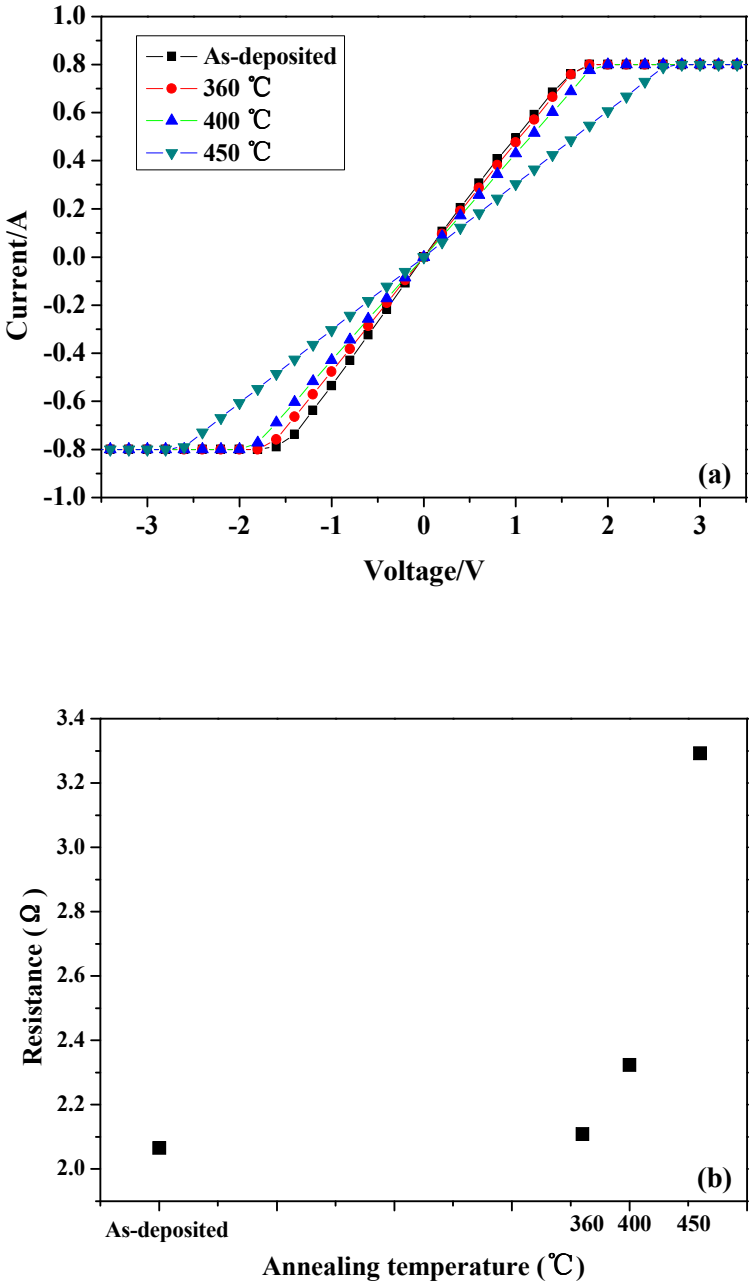

Fig.7 In_2O_3-3 contacts to H_2-cleaned n-InP substrates in terms of different post-deposition annealing temperatures, (a) I-V curve measurements; (b) Calculated dynamic resistances.

Table 1 Parameters of In_2O_3 films deposition by IAD

Main Beam						
Forward Power (W)	Beam Voltage (V)	Accelerate Voltage (V)	Beam Current (mA)	Argon Neutron (sccm)	Argon Source (sccm)	Oxygen (sccm)
200	1000	160	85	3	10	25
Assisted Beam						
Forward Power (W)	Beam Voltage (V)	Accelerate Voltage (V)	Beam Current (mA)	Argon Neutron (sccm)	Argon Source (sccm)	Oxygen (sccm)
110	150	100	31	3	10	0,3,5,7

Table 2 Bulk material properties of In_2O_3 at different deposition conditions

Deposition Condition (O_2 flow rate)	0	3	5	7
Carrier Concentration (cm^{-3})	8.53×10^{19}	2.13×10^{19}	2×10^{19}	2×10^{17}
Conductivity (S/cm)	355.5	99.9	41.9	0.71
Hall Mobility (cm^2/Vs)	26.1	29.3	13.1	21.5
Complex Refr.Ind.@1550nm (n+ik)	1.84+0.025i	1.952+0.0102i	1.9662+0.0071i	2.01+0.004i
Optical Loss@ 1550nm (cm^{-1})	2061.8	831.1	571.9	320.7
Optical Band Gap (eV)	3.75	3.7	3.68	3.65